

LLM-grounded Diffusion: Enhancing Prompt Understanding of Text-to-Image Diffusion Models with Large Language Models

Long Lian¹

Boyi Li¹

Adam Yala^{1,2}

Trevor Darrell¹

¹UC Berkeley

²UCSF

Abstract

Recent advancements in text-to-image diffusion models have yielded impressive results in generating realistic and diverse images. However, these models still struggle with complex prompts, such as those that involve numeracy and spatial reasoning. This work proposes to enhance prompt understanding capabilities in diffusion models. Our method leverages a pretrained large language model (LLM) for grounded generation in a novel two-stage process. In the first stage, the LLM generates a scene layout that comprises captioned bounding boxes from a given prompt describing the desired image. In the second stage, a novel controller guides an off-the-shelf diffusion model for layout-grounded image generation. Both stages utilize existing pretrained models without additional model parameter optimization. Our method significantly outperforms the base diffusion model and several strong baselines in accurately generating images according to prompts that require various capabilities, *doubling* the generation accuracy across four tasks on average. Furthermore, our method enables instruction-based multi-round scene specification and can handle prompts in languages not supported by the underlying diffusion model. We anticipate that our method will unleash users' creativity by accurately following more complex prompts.¹

1 Introduction

The field of text-to-image generation has witnessed significant advancements, particularly with the emergence of diffusion models. These models have showcased remarkable capabilities in generating realistic and diverse images in response to textual prompts. However, despite the impressive results, diffusion models often struggle to accurately follow complex prompts that require specific capabilities to understand. Fig. 1 shows that Stable Diffusion



Figure 1: (a) Stable Diffusion (Rombach et al., 2022) often struggles to accurately follow prompts that involve negation, numeracy, attribute binding, and spatial relationships. (b) Our method LMD achieves enhanced prompt understanding capabilities and accurately follows these types of prompts.

sion (Rombach et al., 2022) could not generate a certain number of objects or understand negation in the prompt. It also struggles with spatial reasoning or associating attributes correctly with objects.

One potential solution to address this issue is of course to gather a comprehensive multi-modal dataset comprising intricate captions and train a text-to-image diffusion model for enhanced prompt understanding. Nonetheless, this approach presents notable drawbacks. It requires considerable time and resources to curate a diverse and high-quality multi-modal dataset, not to mention the challenges associated with training or fine-tuning a diffusion

¹Project page: <https://llm-grounded-diffusion.github.io>

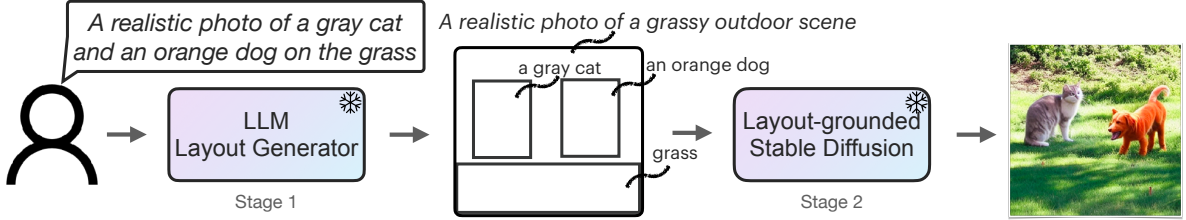


Figure 2: Our proposed LMD enhances prompt understanding in text-to-image diffusion models through a novel two-stage generation process: 1) An LLM layout generator takes a prompt from the user and outputs an image layout in the form of captioned bounding boxes. 2) A stable diffusion model guided by our layout-grounded controller generates the final image. Both stages utilize frozen pretrained models, which makes our method applicable to off-the-shelf LLMs and other diffusion models without grounding in their training objective.

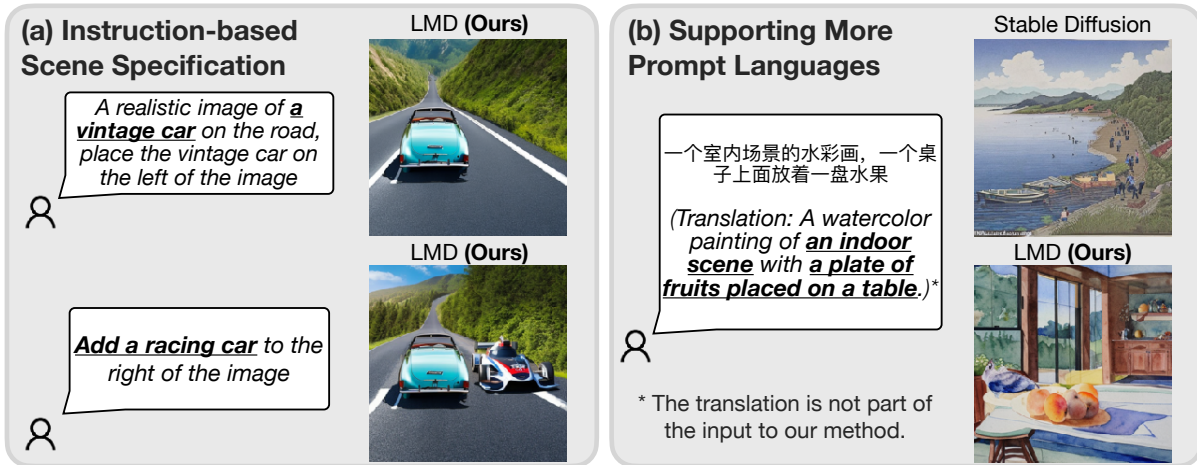


Figure 3: LMD is naturally able to (a) perform instruction-based multi-round scene specification and (b) generate images from prompts in languages not supported by the underlying diffusion model.

model on such extensive data.

In contrast, we propose a novel *training-free* method that equips the diffusion model with an LLM that provides grounding for enhanced prompt understanding. Our method **LMD** consists of a two-stage generation process as shown in Fig. 2.

In the first stage of our method, we adapt an LLM to be a text-grounded layout generator through in-context learning. Given a prompt describing the desired image, the LLM generates scene layouts in the form of captioned bounding boxes, along with a background caption.

In the second stage, we introduce a novel controller that guides an existing diffusion model without grounding in its training objective (e.g., Stable Diffusion) to follow the layout grounding generated in the first stage. In contrast to previous and concurrent works on region control (e.g., Bar-Tal et al. (2023); Chen et al. (2023); Xie et al. (2023)) that apply *semantic* control to certain spatial regions, our approach allows precise control over object *instances* in designated regions.

Notably, both stages utilize frozen pretrained models *off-the-shelf*, making our method applicable to LLMs and diffusion models trained independently *without any LLM or diffusion model parameter optimization*.

In addition to enhanced prompt understanding, our method also enables instruction-based multi-round scene specification (Fig. 3(a)) and image generation from prompts in languages not supported by the base diffusion model (Fig. 3(b)).

As shown in Fig. 1, our LMD provides a unified solution to several caveats in prompt understanding *at once* and enables accurate and high-quality image generation from complex prompts. We demonstrate that a diffusion model, grounded with an LLM-generated layout using LMD, outperforms its base diffusion model and several strong baselines, *doubling* the average generation accuracy across four benchmarks.

Our work makes four main contributions:

1. We improve prompt understanding in text-to-image diffusion models by leveraging LLMs in

a training-free two-stage generation process.

2. We introduce a novel controller that steers a diffusion model to generate images grounded on bounding box layouts from the LLM.
3. LMD enables instruction-based scene specification and allows broader language support for the input prompt.
4. We propose a benchmark to assess the prompt-following ability of a text-to-image model and demonstrate the superior performance of LMD.

We expect LMD to empower users with more precise control of text-to-image diffusion models. [Our code and benchmark have been released](#).

2 Related Work

Text-to-image diffusion models. High-quality image generation from textual descriptions has been popular (Ramesh et al., 2022; Saharia et al., 2022; Rombach et al., 2022), especially with Latent/Stable Diffusion (Rombach et al., 2022) that proposed denoising in the latent space and decoding the denoised latents to high-resolution pixel space. However, these models tends to exhibit subpar performance when it comes to complex prompts that require skills such as binding attributes to objects and spatial reasoning (Ramesh et al., 2022).

Similar to our instruction-based scene specification, Brooks et al. (2023) recently proposed instruction-based image editing with diffusion models. Wu et al. (2023) and Gupta and Kembhavi (2023) also allow using external image editing models in an LLM-driven dialog. Different from these methods, we aim to edit the *scene layout* rather than the *image pixels*, which easily allows a greater set of instructions such as swapping/moving objects. We refer readers to Appendix A for a brief introduction to diffusion models.

LLMs for visual grounding. Many multimodal models benefit from integrating LLMs for grounding vision models. BLIP (Li et al., 2023a) bootstraps vision-language pre-training from frozen image encoders and LLMs. Flamingo (Alayrac et al., 2022) tackles tasks such as few-shot visual question-answering and captioning tasks. Beyond, Rozanova et al. (2021) finds that document-based models can learn a reasonable amount of spatially relevant features that make them transferable to the UI grounding task. Ghanimifard and Dobnik (2019) reveals that the language model pos-

sesses the capability to differentiate between the functional and geometric biases of spatial relations through encoding, despite lacking access to visual features of the scene. Gupta et al. (2021) uses Transformer (Vaswani et al., 2017) for layout prediction, but it focuses on generating layouts for a limited closed set of object classes in the annotated training set.

Spatially-conditioned image generation creates new content based on given prior visual knowledge such as pose, segmentation map, stroke, and layout. Prior to the popularity of diffusion models, SPADE (Park et al., 2019), BlobGAN (Epstein et al., 2022), and Layout2Im (Zhao et al., 2019) synthesize photorealistic images by a given layout. Xu et al. (2017); Johnson et al. (2018); Herzig et al. (2020) generate images with scene graphs. ControlNet (Zhang and Agrawala, 2023), GLIGEN (Li et al., 2023b) and ReCo (Yang et al., 2023) propose training-based adaptation on the diffusion models for spatially-conditioned image generation. However, these methods *rely on annotated external datasets* such as COCO (Lin et al., 2014) to supply images with annotations such as boxes and captions. Furthermore, training-based adaptation not only makes the model incompatible to add-ons such as pretrained LoRA (Hu et al., 2021) weights but also renders it difficult to train a new LoRA model, since the adapted model requires additional spatial annotations for LoRA training set.

In contrast, we propose a training-free generation controller that steers *existing* text-to-image diffusion models that are *not specifically trained* for layout-grounded image generation and does *not* require external datasets. Furthermore, our method can also integrate with training-based methods for further improvements.

Very recently, Bar-Tal et al. (2023); Avrahami et al. (2023); Chen et al. (2023) allow training-free region control in image generation and share a similar task formulation with our layout-to-image stage. However, both works ground the image generation on the *semantics* of the region and pose little control over the number of object instances inside one semantic region, whereas our method focuses on grounding generation on object *instances*.

3 LLM-grounded Diffusion

In this section, we introduce our method LLM-grounded Diffusion (LMD). LMD focuses on the standard text-to-image generation setting: gener-

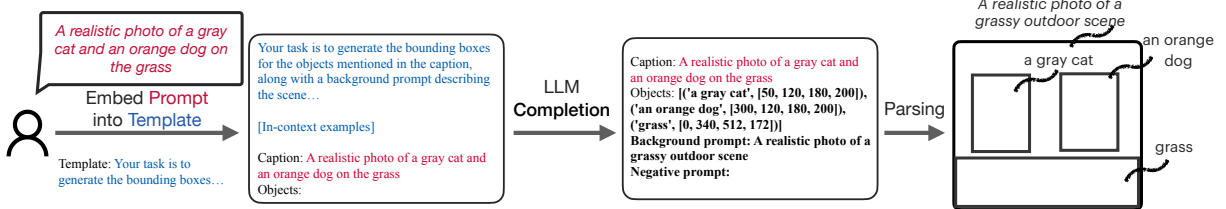


Figure 4: In stage 1, to generate an image layout from a user **prompt**, we first embed the user **prompt** into a **template** with instructions and in-context examples. We then query a frozen LLM for **completion**. Finally, we parse the LLM **completion** to obtain a set of captioned bounding boxes and a background caption.

ate image \mathbf{x}_0 given text prompt \mathbf{y} , potentially by denoising from an initial latent noise \mathbf{z}_T to \mathbf{z}_0 and decoding to pixel space. Our method generates an image in two stages: text-grounded layout generation (Section 3.1) and layout-grounded image generation (Section 3.2).

3.1 LLM-based Layout Generation

To generate the layout of an image, our method embed the input text prompt \mathbf{y} into a template and query the LLM for completion (Fig. 4).

Layout representation of LMD comprises two components: 1) a captioned bounding box for each foreground object, with coordinates specified in the $(x, y, width, height)$ format, and 2) a simple and concise caption describing the image background along with a negative prompt indicating what should not appear in a generated image. The negative prompt is empty when the layout does not impose restrictions on what should not appear.

Prompting. Our prompt to LLM has two parts:

1. Task specification:

Your task is to generate the bounding boxes for the objects mentioned in the caption, along with a background prompt describing the scene.

2. Supporting details:

The images are of size 512x512... Each bounding box should be in the format of ... If needed, you can make reasonable guesses.

In-context learning. Similar to [Brooks et al. \(2023\)](#), we provide the LLM with manually curated examples after the task description. Through these examples, we clarify the layout representation and provide preferences to disperse ambiguity.

An example is shown as follows:

*Caption: A watercolor painting of a wooden table in the living room with an apple on it
Objects: [('a wooden table', [65, 243, 344, 206]), ('an apple', [206, 306, 81, 69])]
Background prompt: A watercolor painting of a living room
Negative prompt:*

To ensure precise layout control, we adhere to two key principles in our example design: 1) Each object instance is represented by a single bounding box. For instance, if the prompt mentions four apples, we include four boxes with the word "apple" included in the caption. 2) We leave no foreground objects specified in the boxes to the background caption to ensure all foreground objects are controlled by our layout-grounded image generator (Section 3.2). These principles allow for accurate and controlled layout generation.

LLM completion. After providing examples, we prompt the LLM for completion²:

*Caption: [input prompt from the user]
Objects: [start of LLM completion]*

The resulting layout from the LLM completion is then parsed and used for the subsequent image generation process. We refer readers to the Appendix F for our complete prompt.

3.2 Layout-grounded Stable Diffusion

In this stage, we introduce a controller to ground the image generation on the LLM-generated layout. While previous training-free region control methods ([Bar-Tal et al., 2023](#); [Chen et al., 2023](#)) apply *semantic* guidance through regional latent denoising or attention manipulation, these methods lack the ability to control the number of objects within a semantic region. This limitation arises as the different instances are often indistinguishable in either

²We use [Text Completion/Chat Completion API](#) to query the LLM for completion.

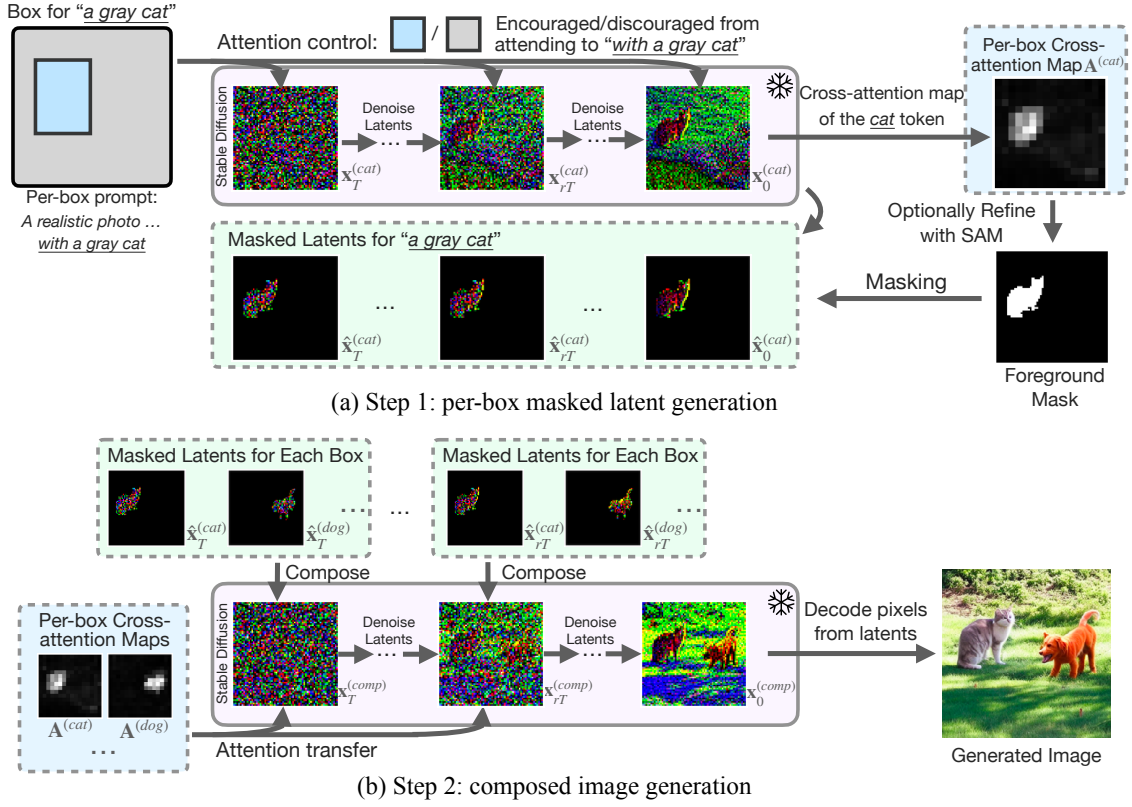


Figure 5: In stage 2, we introduce a novel layout-grounded controller that guides stable diffusion to generate images based on the layout obtained from the previous stage. Our layout-grounded image generation process consists of two steps: **(a)** generating masked latents for each box specified in the layout, with attention control ensuring that the object is placed in the designated box; and **(b)** composing the masked latents coherently to generate images that adhere to the specified foreground boxes and background caption.

the latent space or the attention map, hindering the control over object instances.

In contrast, LMD enables *instance*-level grounding by first generating masked latents for each individual bounding box and then composing the masked latents for overall image generation. This allows for precise placement and attribute binding for each object instance.

Per-box masked latents. While diffusion models lack inherent instance-level distinction in their latent space or attention maps for fine-grained control, we observe that they can generate images with one specified instance. Hence, we process one foreground box at a time for instance-level grounding.

As depicted in Fig. 5(a), for each foreground object i , we first generate an image with a single instance by denoising from $\mathbf{z}_T^{(i)}$ to $\mathbf{z}_0^{(i)}$, where we use “[background prompt] with [box caption]” (e.g., “*a realistic image of an indoor scene with a gray cat*”) as the denoising prompt. The initial noise latent is shared for all boxes to ensure globally coherent viewpoint, style, and lighting (i.e., $\mathbf{z}_T^{(i)} = \mathbf{z}_T, \forall i$).

To ensure the object aligns with the bounding box, we manipulate the cross-attention maps $\mathbf{A}^{(i)}$

of the noise-prediction network.³ Each map describes the affinity from pixels to text tokens:

$$\mathbf{A}_{uv}^{(i)} = \text{Softmax}(\mathbf{q}_u^T \mathbf{k}_v) \quad (1)$$

where \mathbf{q}_u and \mathbf{k}_v are linear transformations of the image feature at spatial location u and the text feature at token index v in the prompt, respectively.

Following Chen et al. (2023); Xie et al. (2023), we strengthen the cross-attention from pixels inside the box to tokens associated with the box caption while attenuating the cross-attention from pixels outside the box. To achieve this, we define a simple energy function:

$$E(\mathbf{A}^{(i)}, i, v) = -\text{Topk}_u(\mathbf{A}_{uv} \cdot \mathbf{m}_i) + \quad (2)$$

$$\omega \text{Topk}_u(\mathbf{A}_{uv} \cdot (1 - \mathbf{m}_i)) \quad (3)$$

where \cdot is element-wise multiplication, \mathbf{m}_i is a binary mask of the box i with the region in the box set to 1, Topk_u takes the average of top-k values across the spatial dimension u , and $\omega = 4.0$. The energy function is minimized by updating the latent

³The cross-attention layer index is omitted for simplicity. We sum the energy values for all layers during optimization.

before each denoising step:

$$\mathbf{z}_t^{(i)} \leftarrow \mathbf{z}_t^{(i)} - \eta \nabla_{\mathbf{z}_t^{(i)}} \sum_{v \in V} E(\mathbf{A}^{(i)}, i, v) \quad (4)$$

$$\mathbf{z}_{t-1}^{(i)} \leftarrow \text{Denoise}(\mathbf{z}_t^{(i)}) \quad (5)$$

where η is the strength hyperparam, and the set V contains the token indices for the box caption in the prompt.

After generation, we obtain the cross-attention map that corresponds to the box caption, which serves as a saliency mask for the object. We optionally use SAM (Kirillov et al., 2023) to refine the quality of the mask. This can be done by querying either with the pixel location that has the highest saliency value or with the layout box.⁴ With mask $m^{(i)}$ for exactly one foreground instance, we perform element-wise multiplication between the mask and the latent at each denoising step:

$$\hat{\mathbf{z}}_t^{(i)} = \mathbf{z}_t^{(i)} \otimes m^{(i)} \quad (6)$$

Composed image generation. As illustrated in Fig. 5(b), at each denoising time step t , we place each masked foreground latents $\hat{\mathbf{z}}_t^{(i)}$ onto the composed latents $\mathbf{z}_t^{(\text{comp})}$, replacing the original content in the masked region:

$$\mathbf{z}_t^{(\text{comp})} \leftarrow \text{Compose}(\mathbf{z}_t^{(\text{comp})}, \hat{\mathbf{z}}_t^{(i)}) \quad \forall i \quad (7)$$

where $\mathbf{z}_T^{(\text{comp})}$ is initialized from \mathbf{z}_T for foreground generation for consistency.

We further transfer the cross-attention maps from per-box generation to the corresponding regions in the composed generation to enhance instance-level guidance through adapting the energy function:

$$E^{(\text{comp})}(\mathbf{A}^{(\text{comp})}, \mathbf{A}^{(i)}, i, v) = E(\mathbf{A}^{(i)}, i, v) + \lambda \sum_{u \in B_i} \left| \mathbf{A}_{uv}^{(\text{comp})} - \mathbf{A}_{uv}^{(i)} \right| \quad (8)$$

where $\lambda = 2.0$ and the energy value of each box i is summed up for optimization.

Diffusion models tend to generate object placement in the initial denoising steps and then refine the details in later steps (Bar-Tal et al., 2023). Taking this into consideration, we only compose the latents from timestep T to rT , where $r \in [0, 1]$ balances instance control and image coherency. By primarily intervening during the steps for object placement, our method allows the diffusion model to optimize for more coherent generation (e.g., making adjustments to match the interactions) while still adhering to the instance specification.

⁴The precision of instance masks could be further improved by using an open vocabulary instance segmentation model with box captions as queries. We leave this to future research.

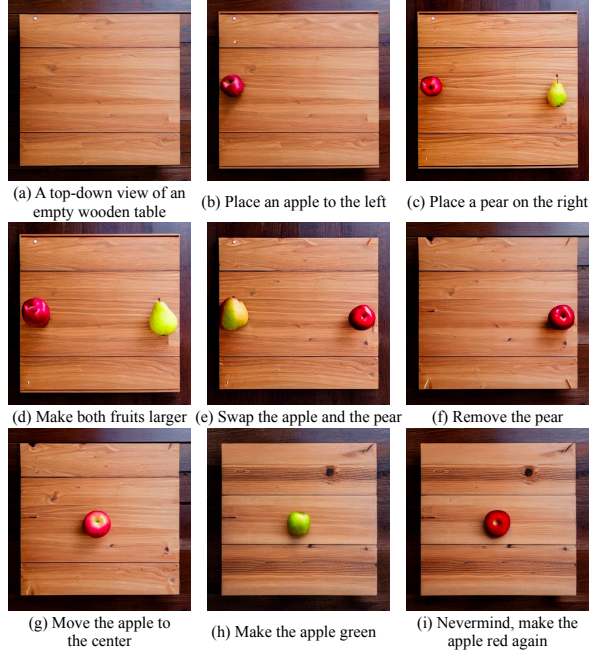


Figure 6: LMD supports instruction-based scene specification, empowering the users to add/move/remove objects and modify object attributes in multiple rounds of dialog. (a): the initial prompt for the scene; (b)-(i): eight subsequent instructions that *sequentially* modify the scene. By separating the generation of each foreground object as well as the background, LMD ensures consistent image generation when the same seed is used for image generation throughout the dialog.

Finally, we decode latents $\mathbf{z}_0^{(\text{comp})}$ to pixels \mathbf{x}_0 via the diffusion image decoder. Please refer to Appendix B for the pseudo-code for layout-grounding.

Integration with training-based methods. Our training-free guidance method can also be integrated with training-based methods such as GLIGEN (Li et al., 2023b) to leverage instance-annotated external datasets when available. GLIGEN inserts and trains adapter layers taking box inputs. The integration with GLIGEN, denoted as LMD+, involves adopting its adapter weights and passing the layout guidance to the adapter layers. Note that LMD+ uses adapters along with the cross-attention guidance introduced above, which greatly surpasses using only the GLIGEN adapters, as shown in Table 2. We achieve further enhanced instance and attribute control without additional training through this integration.

3.3 Additional Capabilities of LMD

Our LLM-grounded generation pipeline allows for two additional capabilities.

Instruction-based scene specification. Leveraging an LLM that supports multi-round dialog (e.g.,

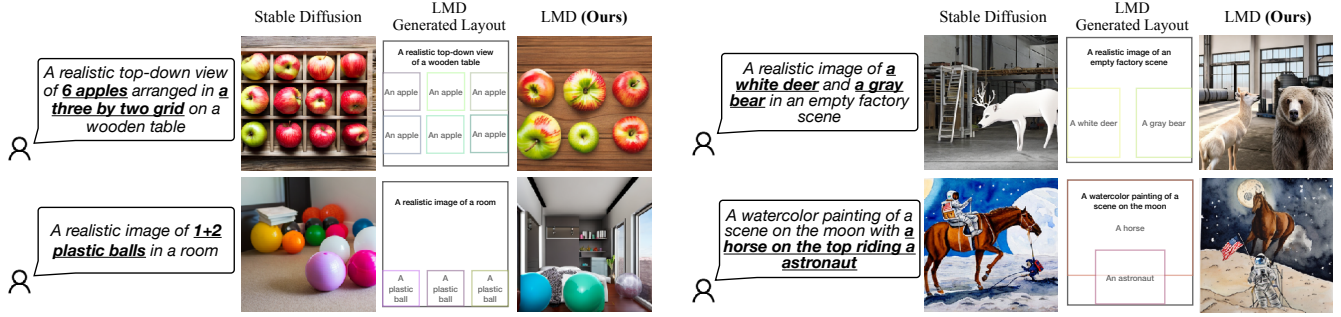


Figure 7: LMD outperforms its base text-to-image diffusion model (Rombach et al., 2022) in accurately following the prompts that require spatial and language reasoning. Best viewed when zoomed in.

GPT-3.5/4), LMD empowers the users to specify the desired image with multiple instructions following an initial prompt (Fig. 3(a)). Specifically, after the initial image generation, users can simply instruct the LLM to update the layout and then generate images with the updated layout. Since we edit the layout rather than the raw image, our generation remains consistent after multiple rounds of requests and can handle requests, such as swapping objects, that were unachievable through previous instruction-based image editing method Brooks et al. (2023), as demonstrated in Fig. 6. This capability applies to both LMD and LMD+.

Supporting more languages. By giving an in-content example of a non-English user prompt and English captions⁵, the LLM layout generator accepts non-English user prompts and outputs layouts with English captions. This allows generation from prompts in languages unsupported by the underlying diffusion model *without re-training* (Fig. 3(b)).

4 Evaluation

4.1 Qualitative Comparison

We qualitatively compare our approach with Stable Diffusion (SD, Rombach et al. (2022)), our base model for layout-grounded image generation. SD is chosen as our base model given its strong capabilities and widespread adoption in text-to-image generation research. We use gpt-4 model (OpenAI, 2023) for layout generation for qualitative comparison, unless stated otherwise. In Fig. 7, we observe that our two-stage text-to-image generation approach greatly enhances the prompt understanding compared to our base model by generating images that align with the LLM-generated layouts.

⁵We simply translate the input prompt of our last in-context example, while keeping the layout captions in English.

Tasks	SD	Accuracy	
		LMD	LMD+
Negation	28%	100% (3.6×)	100% (3.6×)
Generative Numeracy	39%	62% (1.6×)	86% (2.2×)
Attribute Binding	52%	65% (1.3×)	69% (1.3×)
Spatial Relationships	28%	79% (2.8×)	67% (2.4×)
Average	37%	77% (2.1×)	81% (2.2×)

Table 1: With guidance from the LLM-based layout generator and our novel layout-grounded controller, our LMD significantly outperforms the Stable Diffusion model (SD, Rombach et al. (2022)) that we use under the hood in four tasks that benchmark prompt understanding. LMD represents our method directly applied on SD. LMD+ denotes additionally integrating GLIGEN (Li et al., 2023b) into our controller without additional training.

We also compare with *semantic*-controlled image generation methods in Appendix C. Our method shows superior *instance*-level control while still being *training-free*.

4.2 Quantitative evaluation

Benchmark. We propose a text-to-image evaluation benchmark that includes four tasks: negation, generative numeracy, attribute binding, and spatial reasoning. Negation and generative numeracy involve generating a specific number of objects. Attribute binding involves assigning the right attribute to the right object. Spatial reasoning involves understanding words that describe the relative locations of objects. For each task, we programmatically compose 100 prompts and query each model for text-to-image generation. gpt-3.5-turbo (Brown et al., 2020) is used in LMD for the benchmarks. We also implemented a LMD variant that integrates GLIGEN (Li et al.,

Stage 1/Stage 2	Accuracy				
	Negation	Numeracy	Attribute	Spatial	Average
<i>Training-free methods:</i>					
LMD/MultiDiffusion (Bar-Tal et al., 2023)	100%	30%	42%	36%	52.0%
LMD/Backward Guidance (Chen et al., 2023)	100%	42%	36%	61%	59.8%
LMD/BoxDiff (Xie et al., 2023)	100%	32%	55%	62%	62.3%
LMD/LMD (Ours)	100%	62%	65%	79%	76.5% (+ 14.2)
<i>Training-based methods:</i>					
LMD/GLIGEN (Li et al., 2023b)	100%	57%	57%	45%	64.8%
LMD/LMD+ (Ours)	100%	86%	69%	67%	80.5% (+ 15.7)
LMD/LMD+ (Ours, GPT-4)	100%	84%	79%	82%	86.3% (+ 21.5)
<i>Evaluating generated layouts only (upper bound for image generation):</i>					
LMD/-	100%	97%	100%	99%	99.0%

Table 2: Our LLM layout generator (stage 1) is compatible with other layout-to-image methods as stage 2, although our proposed layout-grounded controller performs the best among them. Our controller could also be integrated with training-based Li et al. (2023b), denoted as LMD+, for additional improvements. Finally, the LLM-generated layouts almost always align with the prompt, highlighting that the bottleneck is the layout-grounded image generation. The scores for negation task are high because we pass the negative prompt generated by the LLM to the underlying diffusion model, which does not depend on the stage 2 implementation.

Image (Layout) Accuracy	
Stage 1 Model	Average (4 tasks)
StableBeluga2	67.0% (96.0%)
gpt-3.5-turbo	80.5% (99.0%)
gpt-4	86.3% (100.0%)

Table 3: Ablations on different LLMs in stage 1.

2023b) into our controller without further training and denote it as LMD+. We refer readers to the appendix for implementation details.

Detection-based evaluation. We use an open-vocabulary object detector, OWL-ViT (Minderer et al., 2022), to obtain bounding boxes for the objects of interest. We then check whether each generated image satisfies the requirements in the prompt. The accuracy of each task is computed by calculating the proportion of the image generations that match the prompt over all generations.

Results. As presented in Table 1, our model shows significant improvements in generation accuracy, ranging from $1.3\times$ to $3.6\times$ compared to SD across four tasks and *doubling* the accuracy on average. Notably, LMD achieves image generation accuracy that is *more than twice* of the SD accuracy for the spatial relationships and the negation task. This highlights the utility of the grounding image generation on the LLM layout generator. Further-

more, when adding GLIGEN to our pipeline with attention-based control and leveraging in-domain instance-annotated data, denoted as LMD+, our method achieves additional improvements.

4.3 Ablation Study

Layout-to-image stage. As shown in Table 2, compared with training-free *semantic* control methods, our proposed layout-grounded controller provides much better *instance*-level grounding. Notably, our controller even *surpasses training-based method GLIGEN* (Li et al., 2023b) in attribute binding and spatial reasoning task. When integrated with GLIGEN to leverage instance-annotated datasets, our integration, denoted as LMD+, allows for further improvements without the need for additional training. We also provide an **ablation on the base diffusion model in Appendix E**: Thanks to our training-free nature, LMD maintain the gains to the base model ($2\times$ performance boost) when we switch the base diffusion model from SDv1.5 to SDv2.1 *without hyperparam tuning*. This showcases the potential of integrating LMD with future diffusion models.

Text-to-layout stage. We explored LLM selections in Table 3. All LLMs generate layouts that almost perfectly follow the requirements in the prompts, indicating the bottleneck to be the layout-to-image stage. gpt-4 shows improved results in layout

and the subsequent image generation, compared to gpt-3.5-turbo. The capability to generate high-quality layouts are not limited to proprietary LLMs, with Llama2-based StableBeluga2 (Mahan et al.; Touvron et al., 2023; Mukherjee et al., 2023) also able to perform text-to-layout generation in the stage 1.

5 Summary

In this paper, we aim to enhance the prompt understanding capabilities of text-to-image diffusion models. We present a novel training-free two-stage generation process that incorporates LLM-based text-grounded layout generation and layout-grounded image generation. Our method also enables instruction-based scene specification and generation from prompt in languages unsupported by the base diffusion model. Our method outperforms strong baselines in accurately following the prompts in text-to-image generation.

6 Limitations

Since we use off-the-shelf models without joint fine-tuning, the LLM may generate a layout with ambiguity and may be confusing to the diffusion model. The LLM may also output a layout that the diffusion model is not good at generating. For example, the generated layout in Fig. 8 is feasible for a close-up image, but the diffusion model generates an image viewing from far away, resulting in disproportionate objects and background. A better format for expressing the layout (e.g., scene graph) and using layouts obtained from bounding box detections as in-context examples may alleviate the problem. Furthermore, partially occluded instances in the single-instance generation stage may lead to incomplete foreground objects in the composed generation.

Although our method did not generate coherent images in cases like Fig. 8, our method still offers more interpretability for diagnosis compared to our base model. The user can inspect the layout generated in the first stage to determine whether the unsatisfying generation is due to the text-to-layout stage or the layout-to-image stage and selectively re-run with another random seed or manually tweak the boxes or the captions in the layout for desired generation. In contrast, stable diffusion baseline does not offer insights on why it generates two red apples when the prompt specifies both apples to be green, not to mention providing measures for

fine-grained manipulation and control to achieve desired image generation.

Our method also inherits biases from the Stable Diffusion model. These biases have been analyzed in prior works (Luccioni et al., 2023).

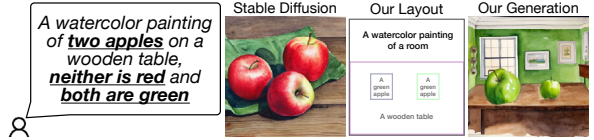


Figure 8: A failure case occurs when our method generates objects that are disproportionate to the background due to layout ambiguity. The LLM-generated layout is suitable for a close-up image, but the layout-to-image model interprets it as viewed from far away.

References

Jean-Baptiste Alayrac, Jeff Donahue, Pauline Luc, Antoine Miech, Iain Barr, Yana Hasson, Karel Lenc, Arthur Mensch, Katherine Millican, Malcolm Reynolds, et al. 2022. Flamingo: a visual language model for few-shot learning. *Advances in Neural Information Processing Systems*, 35:23716–23736.

Omri Avrahami, Thomas Hayes, Oran Gafni, Sonal Gupta, Yaniv Taigman, Devi Parikh, Dani Lischinski, Ohad Fried, and Xi Yin. 2023. Spatext: Spatio-textual representation for controllable image generation. In *Proceedings of the IEEE/CVF Conference on Computer Vision and Pattern Recognition*, pages 18370–18380.

Omer Bar-Tal, Lior Yariv, Yaron Lipman, and Tali Dekel. 2023. Multidiffusion: Fusing diffusion paths for controlled image generation. *arXiv preprint arXiv:2302.08113*, 2.

Tim Brooks, Aleksander Holynski, and Alexei A Efros. 2023. Instructpix2pix: Learning to follow image editing instructions. In *Proceedings of the IEEE/CVF Conference on Computer Vision and Pattern Recognition*, pages 18392–18402.

Tom Brown, Benjamin Mann, Nick Ryder, Melanie Subbiah, Jared D Kaplan, Prafulla Dhariwal, Arvind Neelakantan, Pranav Shyam, Girish Sastry, Amanda Askell, et al. 2020. Language models are few-shot learners. *Advances in neural information processing systems*, 33:1877–1901.

Minghao Chen, Iro Laina, and Andrea Vedaldi. 2023. Training-free layout control with cross-attention guidance. *arXiv preprint arXiv:2304.03373*.

Prafulla Dhariwal and Alexander Nichol. 2021. Diffusion models beat gans on image synthesis. *Advances in Neural Information Processing Systems*, 34:8780–8794.

Dave Epstein, Taesung Park, Richard Zhang, Eli Shechtman, and Alexei A Efros. 2022. Blobgan: Spatially disentangled scene representations. In *Computer Vision–ECCV 2022: 17th European Conference, Tel Aviv, Israel, October 23–27, 2022, Proceedings, Part XV*, pages 616–635. Springer.

Mehdi Ghanimifard and Simon Dobnik. 2019. What a neural language model tells us about spatial relations. In *Proceedings of the Combined Workshop on Spatial Language Understanding (SpLU) and Grounded Communication for Robotics (RoboNLP)*, pages 71–81.

Kamal Gupta, Justin Lazarow, Alessandro Achille, Larry S Davis, Vijay Mahadevan, and Abhinav Shrivastava. 2021. Layouttransformer: Layout generation and completion with self-attention. In *Proceedings of the IEEE/CVF International Conference on Computer Vision*, pages 1004–1014.

Tanmay Gupta and Aniruddha Kembhavi. 2023. Visual programming: Compositional visual reasoning without training. In *Proceedings of the IEEE/CVF Conference on Computer Vision and Pattern Recognition*, pages 14953–14962.

Roei Herzig, Amir Bar, Huijuan Xu, Gal Chechik, Trevor Darrell, and Amir Globerson. 2020. Learning canonical representations for scene graph to image generation. In *Computer Vision–ECCV 2020: 16th European Conference, Glasgow, UK, August 23–28, 2020, Proceedings, Part XXVI 16*, pages 210–227. Springer.

Jonathan Ho, Ajay Jain, and Pieter Abbeel. 2020. Denoising diffusion probabilistic models. *Advances in Neural Information Processing Systems*, 33:6840–6851.

Edward J Hu, Yelong Shen, Phillip Wallis, Zeyuan Allen-Zhu, Yuanzhi Li, Shean Wang, Lu Wang, and Weizhu Chen. 2021. Lora: Low-rank adaptation of large language models. *arXiv preprint arXiv:2106.09685*.

Justin Johnson, Agrim Gupta, and Li Fei-Fei. 2018. Image generation from scene graphs. In *Proceedings of the IEEE conference on computer vision and pattern recognition*, pages 1219–1228.

Alexander Kirillov, Eric Mintun, Nikhila Ravi, Hanzi Mao, Chloe Rolland, Laura Gustafson, Tete Xiao, Spencer Whitehead, Alexander C. Berg, Wan-Yen Lo, Piotr Dollár, and Ross Girshick. 2023. Segment anything. *arXiv:2304.02643*.

Junnan Li, Dongxu Li, Silvio Savarese, and Steven Hoi. 2023a. Blip-2: Bootstrapping language-image pre-training with frozen image encoders and large language models. *arXiv preprint arXiv:2301.12597*.

Yuheng Li, Haotian Liu, Qingyang Wu, Fangzhou Mu, Jianwei Yang, Jianfeng Gao, Chunyuan Li, and Yong Jae Lee. 2023b. Glichen: Open-set grounded text-to-image generation. *arXiv preprint arXiv:2301.07093*.

Tsung-Yi Lin, Michael Maire, Serge Belongie, James Hays, Pietro Perona, Deva Ramanan, Piotr Dollár, and C Lawrence Zitnick. 2014. Microsoft coco: Common objects in context. In *Computer Vision–ECCV 2014: 13th European Conference, Zurich, Switzerland, September 6–12, 2014, Proceedings, Part V 13*, pages 740–755. Springer.

Alexandra Sasha Luccioni, Christopher Akiki, Margaret Mitchell, and Yacine Jernite. 2023. Stable bias: Analyzing societal representations in diffusion models. *arXiv preprint arXiv:2303.11408*.

Calvin Luo. 2022. Understanding diffusion models: A unified perspective. *arXiv preprint arXiv:2208.11970*.

Dakota Mahan, Ryan Carlow, Louis Castricato, Nathan Cooper, and Christian Laforte. [Stable beluga models](#).

Matthias Minderer, Alexey Gritsenko, Austin Stone, Maxim Neumann, Dirk Weissenborn, Alexey Dosovitskiy, Aravindh Mahendran, Anurag Arnab, Mostafa Dehghani, Zhuoran Shen, et al. 2022. Simple open-vocabulary object detection with vision transformers. *arXiv preprint arXiv:2205.06230*.

Ron Mokady, Amir Hertz, Kfir Aberman, Yael Pritch, and Daniel Cohen-Or. 2022. Null-text inversion for editing real images using guided diffusion models. *arXiv preprint arXiv:2211.09794*.

Subhabrata Mukherjee, Arindam Mitra, Ganesh Jawa-har, Sahaj Agarwal, Hamid Palangi, and Ahmed Awadallah. 2023. [Orca: Progressive learning from complex explanation traces of gpt-4](#).

OpenAI. 2023. Gpt-4 technical report. *arXiv preprint arXiv:2303.08774*.

Taesung Park, Ming-Yu Liu, Ting-Chun Wang, and Jun-Yan Zhu. 2019. Semantic image synthesis with spatially-adaptive normalization. In *Proceedings of the IEEE/CVF conference on computer vision and pattern recognition*, pages 2337–2346.

Aditya Ramesh, Prafulla Dhariwal, Alex Nichol, Casey Chu, and Mark Chen. 2022. Hierarchical text-conditional image generation with clip latents. *arXiv preprint arXiv:2204.06125*.

Robin Rombach, Andreas Blattmann, Dominik Lorenz, Patrick Esser, and Björn Ommer. 2022. High-resolution image synthesis with latent diffusion models. In *Proceedings of the IEEE/CVF Conference on Computer Vision and Pattern Recognition*, pages 10684–10695.

Olaf Ronneberger, Philipp Fischer, and Thomas Brox. 2015. U-net: Convolutional networks for biomedical image segmentation. In *Medical Image Computing and Computer-Assisted Intervention—MICCAI 2015: 18th International Conference, Munich, Germany, October 5–9, 2015, Proceedings, Part III 18*, pages 234–241. Springer.

Julia Rozanova, Deborah Ferreira, Krishna Dubba, Wei-wei Cheng, Dell Zhang, and Andre Freitas. 2021. Grounding natural language instructions: Can large language models capture spatial information? *arXiv preprint arXiv:2109.08634*.

Chitwan Saharia, William Chan, Saurabh Saxena, Lala Li, Jay Whang, Emily L Denton, Kamayyar Ghasemipour, Raphael Gontijo Lopes, Burcu Karagol Ayan, Tim Salimans, et al. 2022. Photo-realistic text-to-image diffusion models with deep language understanding. *Advances in Neural Information Processing Systems*, 35:36479–36494.

Jiaming Song, Chenlin Meng, and Stefano Ermon. 2020. Denoising diffusion implicit models. *arXiv preprint arXiv:2010.02502*.

Hugo Touvron, Louis Martin, Kevin Stone, Peter Albert, Amjad Almahairi, Yasmine Babaei, Nikolay Bashlykov, Soumya Batra, Prajjwal Bhargava, Shruti Bhosale, Dan Bikel, Lukas Blecher, Cristian Canton Ferrer, Moya Chen, Guillem Cucurull, David Esiobu, Jude Fernandes, Jeremy Fu, Wenjin Fu, Brian Fuller, Cynthia Gao, Vedanuj Goswami, Naman Goyal, Anthony Hartshorn, Saghar Hosseini, Rui Hou, Hakan Inan, Marcin Kardas, Viktor Kerkez, Madian Khabsa, Isabel Kloumann, Artem Korenev, Punit Singh Koura, Marie-Anne Lachaux, Thibaut Lavril, Jenya Lee, Diana Liskovich, Yinghai Lu, Yuning Mao, Xavier Martinet, Todor Mihaylov, Pushkar Mishra, Igor Molybog, Yixin Nie, Andrew Poulton, Jeremy Reizenstein, Rashi Rungta, Kalyan Saladi, Alan Schelten, Ruan Silva, Eric Michael Smith, Ranjan Subramanian, Xiaoqing Ellen Tan, Binh Tang, Ross Taylor, Adina Williams, Jian Xiang Kuan, Puxin Xu, Zheng Yan, Iliyan Zarov, Yuchen Zhang, Angela Fan, Melanie Kambadur, Sharan Narang, Aurelien Rodriguez, Robert Stojnic, Sergey Edunov, and Thomas Scialom. 2023. [Llama 2: Open foundation and fine-tuned chat models](#).

Ashish Vaswani, Noam Shazeer, Niki Parmar, Jakob Uszkoreit, Llion Jones, Aidan N Gomez, Łukasz Kaiser, and Illia Polosukhin. 2017. Attention is all you need. *Advances in neural information processing systems*, 30.

Chenfei Wu, Shengming Yin, Weizhen Qi, Xiaodong Wang, Zecheng Tang, and Nan Duan. 2023. Visual chatgpt: Talking, drawing and editing with visual foundation models. *arXiv preprint arXiv:2303.04671*.

Jinheng Xie, Yuexiang Li, Yawen Huang, Haozhe Liu, Wentian Zhang, Yefeng Zheng, and Mike Zheng Shou. 2023. Boxdiff: Text-to-image synthesis with training-free box-constrained diffusion. *arXiv preprint arXiv:2307.10816*.

Danfei Xu, Yuke Zhu, Christopher B Choy, and Li Fei-Fei. 2017. Scene graph generation by iterative message passing. In *Proceedings of the IEEE conference on computer vision and pattern recognition*, pages 5410–5419.

Zhengyuan Yang, Jianfeng Wang, Zhe Gan, Linjie Li, Kevin Lin, Chenfei Wu, Nan Duan, Zicheng Liu, Ce Liu, Michael Zeng, et al. 2023. Reco: Region-controlled text-to-image generation. In *Proceedings of the IEEE/CVF Conference on Computer Vision and Pattern Recognition*, pages 14246–14255.

Lvmin Zhang and Maneesh Agrawala. 2023. Adding conditional control to text-to-image diffusion models. *arXiv preprint arXiv:2302.05543*.

Bo Zhao, Lili Meng, Weidong Yin, and Leonid Sigal. 2019. Image generation from layout. In *Proceedings of the IEEE/CVF Conference on Computer Vision and Pattern Recognition*, pages 8584–8593.

A Preliminary introduction on diffusion models

Diffusion models are a class of powerful generative models that learn the data distribution of complex datasets. During the forward process, noise is added to an image to the input data \mathbf{x}_0 for T steps, until the resulting vector \mathbf{x}_T is almost distributed according to a standard Gaussian distribution. In the reverse process, a diffusion model iteratively subtracts a predicted noise vector from \mathbf{x}_T to transform it into a sample that resembles the real data in the training dataset. The reverse process is often referred to as “denoising”. We refer readers to (Luo, 2022) for a more in-depth introduction to diffusion models.

DDPM. (Ho et al., 2020). The denoising process of denoising diffusion probabilistic models starts with the initial noise vector sampled from a standard Gaussian noise vector $\mathbf{x}_T \sim \mathcal{N}(0, \mathbf{I})$. During training, a neural network with parameter θ learns to predict the added noise for the forward process by minimizing the training objective:

$$\mathcal{L} = \|\epsilon - \epsilon_\theta(\mathbf{x}_t, t)\|^2 \quad (9)$$

At inference time, for each of the T denoising steps, DDPM predicts the noise ϵ and then obtains \mathbf{x}_{t-1} from \mathbf{x}_t :

$$\mathbf{x}_{t-1} = \frac{1}{\sqrt{\alpha_t}} \left(\mathbf{x}_t - \frac{1 - \alpha_t}{\sqrt{1 - \prod_{i=1}^t \alpha_i}} \epsilon_\theta(\mathbf{x}_t, t) \right) + \sigma_t \mathbf{z} \quad (10)$$

where $\mathbf{z} \sim \mathcal{N}(0, \mathbf{I})$, α_t and σ_t are parameterized by a variance schedule $\{\beta_t \in (0, 1)\}_{t=1}^T$ that controls the size of the denoising step.

DDIM (Song et al., 2020). Denoising diffusion implicit models are a generalization to DDPM which allows sampling with fewer iterations. DDIM applies the following update rule:

$$\mathbf{x}_{t-1} = \sqrt{\alpha_{t-1}} \left(\frac{\mathbf{x}_t - \sqrt{1 - \alpha_t} \epsilon_\theta(\mathbf{x}_t, t)}{\sqrt{\alpha_t}} \right) + \sigma_t \epsilon_t \quad (11)$$

Note that DDIM shares the same training procedure with DDIM, which means we can take a model trained with DDPM objective and perform faster sampling using DDIM. When σ_t is set to 0, which is the case for our setting, the denoising becomes deterministic given \mathbf{x}_T . Assuming each step only performs small changes to \mathbf{x}_t , DDIM sampling can also be conducted in the reverse order, as proposed in (Song et al., 2020; Dhariwal and Nichol, 2021) to obtain a vector \mathbf{x}'_T from \mathbf{x}_0 so that \mathbf{x}'_T , when de-noised, gives back \mathbf{x}'_0 that is close to \mathbf{x}_0 . The process of inverting the \mathbf{x}_0 to get \mathbf{x}'_T is called

DDIM inversion (Mokady et al., 2022).

Latent Diffusion and Stable Diffusion (Rombach et al., 2022). While DDIM and DDPM are denoising images from raw pixel space, latent diffusion proposes to denoise from initial latent noise \mathbf{z}_T to \mathbf{z}_0 . Then an image decoder decodes the generated \mathbf{z}_0 in the latent space to an output image \mathbf{x}_0 . Latent/Stable Diffusion lowers the cost of training high resolution diffusion models and is widely used in text-to-image generation. Our method improves the prompt understanding of Stable Diffusion without adapting the weights.

Latent diffusion also proposes a conditioning scheme that allows generating samples with other modalities (e.g., text) as the condition. The condition is realized through cross-attention layers (Vaswani et al., 2017) that attend from latent locations in U-Net (Ronneberger et al., 2015) feature maps to the encoded condition (e.g., text features from a CLIP text encoder).

Stable diffusion models are large text-to-image generation models trained on large multi-modal datasets using the techniques proposed for latent diffusion.

B Pseudo-code for layout-grounded image generation

We present the pseudo-code for our layout-grounding stage (stage 2) in Algorithm 1. We explain the functionality of the functions used in the pseudo-code:

1. `SampleGaussian` samples i.i.d standard Gaussian as the initial noise for the latent tensor.
2. `PromptForBox` simply sets “[background prompt] with [box caption]” (e.g., “a realistic image of an indoor scene with a gray cat”) as the denoising prompt.
3. `AttnControl` performs backward guidance to minimize the energy function described in the main text to encourage the attention to the area within the box and discourage the attention on area outside the box.
4. `Denoise` denotes one denoising step by the diffusion model.
5. `TemporalAverage` averages the cross-attention map across the timestep dimension
6. `SAMRefine` refines the attention map by internally decoding the latent and refining with

Algorithm 1 Layout-grounded image generation.

Input: A set of captioned bounding boxes $\{(\mathbf{b}^{(i)}, \mathbf{y}^{(i)})\}_{i=1}^N$. Background caption $\mathbf{y}^{(\text{bg})}$.
Output: Image $\mathbf{z}^{(\text{comp})}$.

- 1: $\mathbf{z}_T \leftarrow \text{SampleGaussian}(\mathbf{0}, \mathbf{I})$
- 2: *Per-box masked latent generation:*
- 3: **for** each captioned box $(\mathbf{b}^{(i)}, \mathbf{y}^{(i)})$ **do**
- 4: $\mathbf{z}_T^{(i)} \leftarrow \mathbf{z}_T$
- 5: $\mathbf{y}^{(i)} \leftarrow \text{PromptForBox}(\mathbf{y}^{(i)}, \mathbf{y}^{(\text{bg})})$
- 6: **for** $t \leftarrow T$ to 1 **do**
- 7: $\mathbf{z}_t^{(i)} \leftarrow \text{AttnControl}(\mathbf{z}_t^{(i)}, \mathbf{y}^{(i)}, \mathbf{b}^{(i)})$
- 8: $\mathbf{z}_{t-1}^{(i)} \leftarrow \text{Denoise}(\mathbf{z}_t^{(i)}, \mathbf{y}^{(i)})$ with cross-attention map extracted to $A_t^{(i)}$
- 9: **end for**
- 10: $A'^{(i)} \leftarrow \text{TemporalAverage}(A_t^{(i)})$
- 11: $A^{(i)} \leftarrow \text{SAMRefine}(A'^{(i)}, \mathbf{z}_0^{(i)})$ (Optional: can also use thresholding instead)
- 12: **end for**
- 13: *Composed image generation:*
- 14: $\mathbf{z}_T^{(\text{comp})} \leftarrow \mathbf{z}_T$
- 15: $\mathbf{y} \leftarrow \text{ComposedPrompt}((\mathbf{y}^{(i)})_{i=1}^N, \mathbf{y}^{(\text{bg})})$
- 16: **for** $t \leftarrow T$ to 1 **do**
- 17: **if** $t \geq rT$ **then**
- 18: $\mathbf{z}_t^{(\text{comp})} \leftarrow \text{LatentCompose}(\mathbf{z}_t^{(\text{comp})},$
- 19: $(\mathbf{z}^{(i)})_{i=1}^N, A^{(i)})$
- 20: $\mathbf{z}_t^{(\text{comp})} \leftarrow \text{AttnTransfer}(\mathbf{z}_t^{(\text{comp})},$
- 21: $\mathbf{y}^{(\text{comp})}, A_t^{(i)})$
- 22: **end if**
- 23: $\mathbf{z}_{t-1}^{(\text{comp})} \leftarrow \text{Denoise}(\mathbf{z}_t^{(\text{comp})}, \mathbf{y}^{(\text{comp})})$
- 24: **end for**
- 25: $\mathbf{x}_0 \leftarrow \text{Decode}(\mathbf{z}_0^{(\text{comp})})$

SAM. If SAM is not enabled, we perform a thresholding instead.

7. ComposedPrompt composes the prompt for overall generation. We offer two options for the overall prompt: using the original input prompt or composing the prompt as “[background prompt] with [box caption 1], [box caption 2], ...”. The former one allows capturing the object as well as foreground-background interactions that are not captured in the layout. The latter allows captions in languages unsupported by the diffusion model and stays robust when the caption is misleading (e.g., “neither of the apples is red”). We use the latter by default but also allow the former for fine-grained adjustments.

8. LatentCompose spatially composes the latent with respect to the mask, replacing the content of the destination latent on the masked locations.
9. AttnTransfer performs backward guidance to minimize the energy function described in the main text to encourage the attention in overall generation within the box to be similar to the attention in per-box generation.

C Qualitative comparison with semantic-grounded image generation methods

We compare with MultiDiffusion (Bar-Tal et al., 2023) and Chen et al. (2023) which allow semantic-grounded image generation. Since MultiDiffusion and Chen et al. (2023) are proposed to leverage semantic masks as the guidance without a text-to-layout generation stage, we reuse the layout generated in stage 1 of LMD (Fig. 9(b)). We present the first four generated images with no random seed selection. While Stable Diffusion does not adhere to the number of balls in the prompt (Fig. 9(c)), MultiDiffusion and Chen et al. (2023) generate images with *semantics* that match the layout (Fig. 9(d) and (e)) without fine-grained control over the instances. As shown in Fig. 9(f), our method correctly generates three plastic balls in three out of four images, showing better instance-level control.

D Details for text-to-image benchmarks

We pick 10 common object types from the COCO dataset (Lin et al., 2014) for generation⁶.

For negation and generative numeracy task, each prompt requires the model to generate a layout of a scene with some number of a certain object or without a certain object. Then we count the number of objects and consider the layout to be correct if the number of the object of that particular type matches the one in the prompt, with the number ranging from 1 to 5.

The objective for each prompt in the attribute binding task is to generate a object of a color and another object of another color, for which the evaluation is similar to other tasks.

For the spatial relationship task, we generate an object at a certain location and another object at an opposite location (left/right and top/bottom). We

⁶Backpack, book, bottle, bowl, car, cat, chair, cup, dog, and laptop.

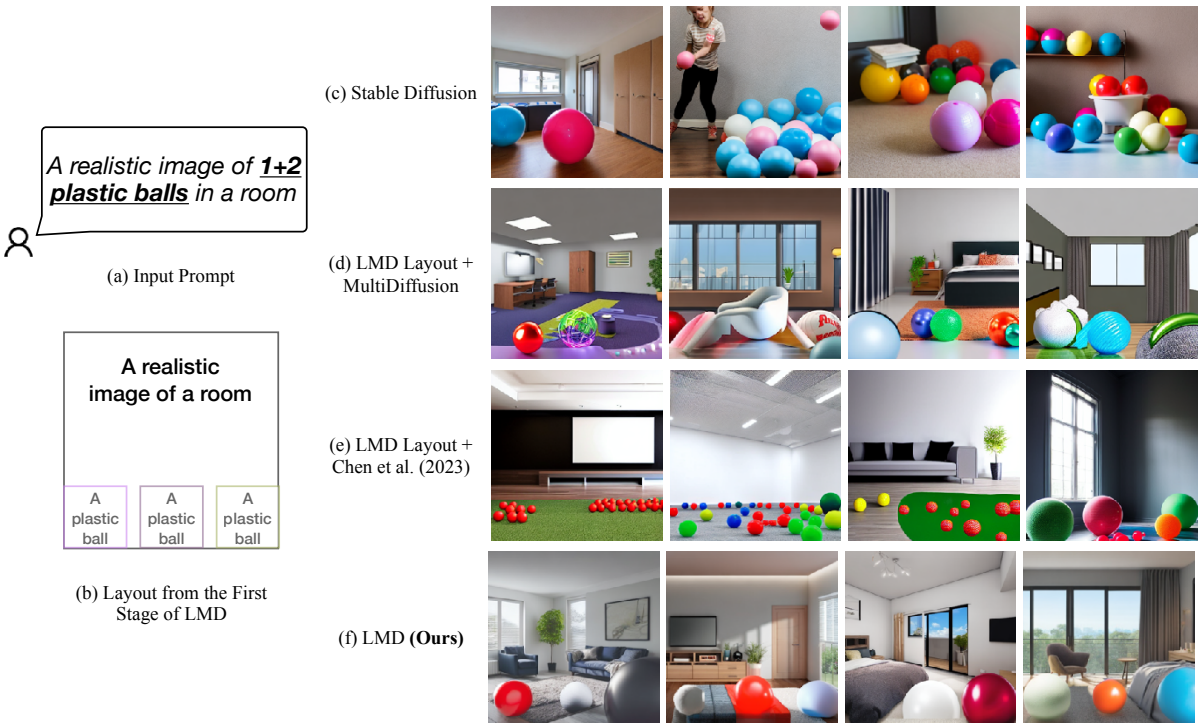


Figure 9: Our layout-grounded image generator has better instance-level control compared to MultiDiffusion (Bar-Tal et al., 2023) and Chen et al. (2023) (backward guidance). While MultiDiffusion and Chen et al. (2023) only specify the semantic regions, our layout-guided image generator specifies one instance at the location of each box. Our method correctly generates exactly one ball for a box in three out of four attempts.

Method	Image Accuracy	
	Average (4 tasks)	
SD v1.5 (Default setting)	37%	
LMD on SD v1.5 (Ours , default setting)	77% (2.1\times)	
SD v2.1	38%	
LMD on SD v2.1 (Ours)	77% (2.0\times)	

Table 4: Our method achieves significant gains when adapted to Stable Diffusion v2.1 as the base model without any hyperparam tuning or model training. The performance of our method could be improved by additional hyperparam tuning. This shows a promising signal that our method could also improve along with the enhancement of diffusion models in the future.

then check the spatial coordinates of the boxes to ensure the layout exactly matches the prompt. In each task, we generate 100 text prompts, with 400 text prompts in total.

Prompts. For the negation benchmark, we use the prompt *A realistic photo of a scene without [object name]*.

For generative numeracy, we use the prompt *A realistic photo of a scene with [number] [object name]*.

For attribute assignment, we use the prompt *A realistic photo of a scene with [modifier 1] [object*

name 1] and [modifier 2] [object name2], where the two modifiers are randomly chosen from colors (red, orange, yellow, green, blue, purple, pink, brown, black, white, gray).

For the spatial relationship benchmark, we use the prompt *A realistic photo of a scene with [object name 1] on the [location] and [modifier 2] [object name2] on the [opposite location]*, where the location is chosen from left, right, top, and bottom.

Implementation details. For LMD, we use Stable Diffusion v1.5 by default. For LMD+, we use GLI-GEN (Li et al., 2023b) model without additional

training or adaptation. We selected the GLIGEN (Li et al., 2023b) model trained based on Stable Diffusion v1.4, which is the latest at the time of writing. We use $\eta = 5$, $\lambda = 2.0$, $r = 0.4$, guidance scale 7.5. The energy minimization is repeated 5 times for each denoising timestep and linearly decrease for every five denoising steps until the repetition is reduced to 1. k in the $\text{Topk}(\cdot)$ in Eq. (3) is set to 20% of the area of the mask for each mask. The the background part (second term) of Eq. (3) is weighted by $\omega = 4.0$. We decouple the scheduler for latent composition and energy minimization, and we only conduct energy minimization during the first 10 iterations of denoising to accelerate generation. The visualizations are generated by LMD by default unless stated otherwise.

E Ablations on different base diffusion models

Unlike training-based methods, our method is applicable to different base diffusion models. As shown in Table 4, our method maintains considerable performance gains when the base diffusion model is switched. Note that we do not perform hyperparam tuning on SDv2.1 and directly use the settings from SDv1.5. Additional hyperparam tuning may further improve the performance.

F Our LLM prompt

Our LLM prompt is listed in Table 5. Our in-context examples are listed in Table 6.

¹ You are an intelligent bounding box generator. I will provide you with a caption for a photo, image, or painting. Your task is to generate the bounding boxes for the objects mentioned in the caption, along with a background prompt describing the scene. The images are of size 512x512. The top-left corner has coordinate [0, 0]. The bottom-right corner has coordinate [512, 512]. The bounding boxes should not overlap or go beyond the image boundaries. Each bounding box should be in the format of (object name, [top-left x coordinate, top-left y coordinate, box width, box height]) and should not include more than one object. Do not put objects that are already provided in the bounding boxes into the background prompt. Do not include non-existing or excluded objects in the background prompt. Use "A realistic scene" as the background prompt if no background is given in the prompt. If needed, you can make reasonable guesses. Please refer to the example below for the desired format.

²

³ [In-context Examples]

⁴

⁵ Caption: [User Prompt]

⁶ Objects:

Table 5: Our full prompt to the LLM for layout generation. LLM starts completion from “Objects:”.

1 Caption: A realistic image of landscape scene depicting a green car parking on the
 left of a blue truck, with a red air balloon and a bird in the sky
 2 Objects: [('a green car', [21, 281, 211, 159]), ('a blue truck', [269, 283, 209,
 160]), ('a red air balloon', [66, 8, 145, 135]), ('a bird', [296, 42, 143,
 100])]
 3 Background prompt: A realistic landscape scene
 4 Negative prompt:
 5
 6 Caption: A realistic top-down view of a wooden table with two apples on it
 7 Objects: [('a wooden table', [20, 148, 472, 216]), ('an apple', [150, 226, 100,
 100]), ('an apple', [280, 226, 100, 100])]
 8 Background prompt: A realistic top-down view
 9 Negative prompt:
 10
 11 Caption: A realistic scene of three skiers standing in a line on the snow near a
 palm tree
 12 Objects: [('a skier', [5, 152, 139, 168]), ('a skier', [278, 192, 121, 158]), ('a
 skier', [148, 173, 124, 155]), ('a palm tree', [404, 105, 103, 251])]
 13 Background prompt: A realistic outdoor scene with snow
 14 Negative prompt:
 15
 16 Caption: An oil painting of a pink dolphin jumping on the left of a steam boat on
 the sea
 17 Objects: [('a steam boat', [232, 225, 257, 149]), ('a jumping pink dolphin', [21,
 249, 189, 123])]
 18 Background prompt: An oil painting of the sea
 19 Negative prompt:
 20
 21 Caption: A cute cat and an angry dog without birds
 22 Objects: [('a cute cat', [51, 67, 271, 324]), ('an angry dog', [302, 119, 211,
 228])]
 23 Background prompt: A realistic scene
 24 Negative prompt: birds
 25
 26 Caption: Two pandas in a forest without flowers
 27 Objects: [('a panda', [30, 171, 212, 226]), ('a panda', [264, 173, 222, 221])]
 28 Background prompt: A forest
 29 Negative prompt: flowers
 30
 31 Caption: An oil painting of a living room scene without chairs with a painting
 mounted on the wall, a cabinet below the painting, and two flower vases on the
 cabinet
 32 Objects: [('a painting', [88, 85, 335, 203]), ('a cabinet', [57, 308, 404, 201]),
 ('a flower vase', [166, 222, 92, 108]), ('a flower vase', [328, 222, 92, 108])]
 33 Background prompt: An oil painting of a living room scene
 34 Negative prompt: chairs

Table 6: Our in-context examples.